Moving mesoscale plasma precipitation in the cusp

S. Taguchi,[1] S. Suzuki,[2,3] K. Hosokawa,[1] Y. Ogawa,[4] A. S. Yukimatu,[4] N. Sato,[4] M. R. Collier,[5] and T. E. Moore[5]

Received 4 February 2009; revised 23 April 2009; accepted 1 May 2009; published 18 June 2009.

[1] On 28 March 2001, when the interplanetary magnetic field was strongly duskward, the DMSP F12 spacecraft observed an ion precipitation burst in a latitudinally narrow region near 1200 MLT. A few minutes earlier, the Low Energy Neutral Atom (LENA) imager on the IMAGE spacecraft, whose field of view (FOV) looks into the high-altitude cusp, detected an enhancement of energetic neutral atom signals, which are produced by the ion injection. The LENA data suggest that the ion injection moved out of its FOV after approximately 4 min. At this time, the ground-based magnetometers of the IMAGE chain in Svalbard, located westward of LENA's FOV, began to indicate perturbations. These perturbations immediately reached a peak and then ceased; the perturbations lasted 2–3 min. During this interval, there was an enhanced westward flow over Svalbard, as observed by the SuperDARN radars. The EISCAT Svalbard radar detected an enhancement of electron density and temperature that was concurrent with this flow enhancement, suggesting that a plasma precipitation burst accompanied with the flow. These observations, which cover a longitudinally extending region of the cusp, strongly suggest the existence of moving mesoscale plasma precipitation (MMPP). The MMPP travels westward with a longitudinally elongated form. Its leading and trailing edges should be created by the temporal effect of the cusp. The other edges, which lie along the streamline, would originate in a spatially limited region along the open-closed line. The boundary of the MMPP form is delineated by both the temporal and spatial structures of the cusp.

Citation: Taguchi, S., S. Suzuki, K. Hosokawa, Y. Ogawa, A. S. Yukimatu, N. Sato, M. R. Collier, and T. E. Moore (2009), Moving mesoscale plasma precipitation in the cusp, *J. Geophys. Res.*, *114*, A06211, doi:10.1029/2009JA014128.

1. Introduction

[2] Ions precipitating into the low-altitude cusp provide important information on how magnetic reconnection occurs on the magnetopause. A typical feature observed in the low-altitude cusp is ion dispersion signatures in which the average ion energy decreases smoothly as the distance from the footprint of the reconnection line increases [e.g., *Reiff et al.*, 1977]. This reflects the fact that the injection occurs in a spatially limited region on the moving flux tubes newly opened by magnetic reconnection [e.g., *Reiff et al.*, 1977; *Menietti and Burch*, 1988; *Onsager et al.*, 1995].

[3] The low-altitude cusp also shows ion signatures with sudden changes in the energy and energy flux instead of smooth dispersion [e.g., *Newell and Meng*, 1991; *Escoubet et al.*, 1992; *Pinnock et al.*, 1995]. The significance of these "stepped" signatures remains a topic of controversy. While these changes can be explained only by temporal variations in the reconnection rate [e.g., *Cowley et al.*, 1991; *Lockwood and Smith*, 1992], i.e., the temporal structure of the cusp, they can be interpreted as a result of crossing the boundary between the spatially separated flux tubes, i.e., the spatial structure of the cusp [e.g., *Weiss et al.*, 1995; *Wing et al.*, 2001; *Trattner et al.*, 2002].

[4] An ion step created by temporal variations in the reconnection should move downstream. Remote sensing techniques for observing the precipitating ions from spacecraft, such as the spectrographic imager SI-12 of the Far-Ultraviolet Instrument (FUV) [*Mende et al.*, 2000] onboard the IMAGE spacecraft, may be used to determine whether the ion step moves. However, it is not easy to detect the motion with velocity 1–2 km s^{-1} from the FUV data alone, because the spatial resolution of the FUV is roughly 100 km at the ionospheric heights and the temporal resolution is 120 s.

[5] Recently, by using simultaneous observations of the FUV proton aurora emissions and energetic neutral atom (ENA) signals detected by the Low Energy Neutral Atom (LENA) Imager [*Moore et al.*, 2000] on IMAGE, *Suzuki et al.* [2008] have reported moving signatures in the cusp proton aurora. As used by *Suzuki et al.* [2008], LENA is known to be capable of detecting ENA emissions produced by ion injection into the cusp through a charge exchange with the Earth's hydrogen exosphere [e.g., *Taguchi et al.*,

[1]Department of Information and Communication Engineering, University of Electro-Communications, Tokyo, Japan.
[2]Sugadaira Space Radio Observatory, University of Electro-Communications, Tokyo, Japan.
[3]Now at National Institute of Polar Research, Tokyo, Japan.
[4]National Institute of Polar Research, Tokyo, Japan.
[5]NASA Goddard Space Flight Center, Greenbelt, Maryland, USA.

Copyright 2009 by the American Geophysical Union.
0148-0227/09/2009JA014128

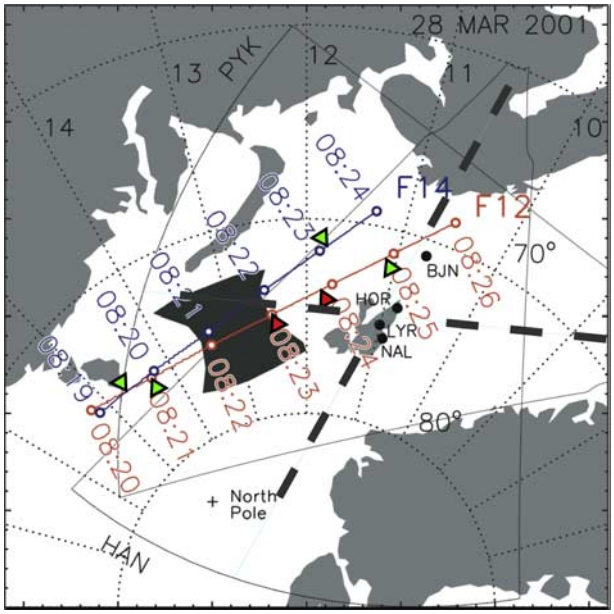

Figure 1. DMSP F12 and F14 passes, the mapped field of view (FOV) of the IMAGE/LENA at 0820 UT (dark gray area in the postnoon sector), and the FOV of the SuperDARN radars at Hankasalmi (HAN), Finland, and Pykkvybaer (PYK), Iceland in the MLAT-MLT coordinate for an ion burst event on 28 March 2001. The geographic map at 0820 UT is overlaid. The interval bounded by the two red triangles along the F12 pass shows the location of the observation of the ion precipitation burst. The green triangles for both passes indicate the equatorward and poleward boundaries of the cusp, which is determined in Figure 2. Dashed line in the FOV of the SuperDARN radar shows the location of the FOV of beam 6 of the PYK radar and beam 9 of the HAN radar, which cover the FOV of the field-aligned beam of the EISCAT Svalbard radar in Longyearbyen (LYR).

2004, 2005, 2006, 2009; *Murata et al.*, 2007] as well as the emissions from the magnetosheath flow near the subsolar magnetopause [*Collier et al.*, 2001a, 2001b, 2005; *Moore et al.*, 2003; *Fok et al.*, 2003; *Hosokawa et al.*, 2008] and the ion outflow from the ionosphere [e.g., *Moore et al.*, 2001; *Wilson and Moore*, 2005; *Nosé et al.*, 2005]. As shown in some of the above studies, the combination of the LENA cusp signal obtained simultaneously with data from other instruments has provided us with insights into the dynamics of the cusp.

[6] In this paper, we report the results of multi-instrument observations of the dayside cusp: ENA signals obtained from IMAGE/LENA, the ion precipitation burst observed by the DMSP spacecraft, convection and related features obtained from the EISCAT Svalbard radar (ESR) and two SuperDARN radars [*Greenwald et al.*, 1995], and the enhanced ionospheric current measured by the ground-based magnetometers of the IMAGE chain [*Syrjaasuo et al.*, 1998]. The ion burst was observed by DMSP F12 in a latitudinally narrow (approximately 100-km wide) region within the cusp. Remote sensing data from IMAGE/LENA, the EISCAT/SuperDARN radars, and the IMAGE magnetometer chain suggest that the ion burst region is accompanied by an enhanced westward flow. We discuss how the temporal and spatial structures of the cusp coexist in this moving plasma precipitation region.

2. Observations

[7] Figure 1 shows the orbit of the DMSP F12 and F14 spacecraft, the mapped field of view (FOV) of IMAGE/LENA at 0820 UT (the dark distorted rectangle in the postnoon sector), and the FOV of the SuperDARN radars at Pykkvybaer (PYK), Iceland (63.86°N, 19.20°E) and Hankasalmi (HAN), Finland (63.32°N, 26.61°E), in the MLAT-MLT coordinates for the event investigated in this study. The bold dashed lines in the FOV of the PYK and HAN radars indicate the crude location of the FOV for beams 6 and 9, respectively; these beams cover the FOV of the ESR at Longyearbyen (LYR), Svalbard. Data from these beams of the SuperDARN radars and the field-aligned beam of the ESR are shown later.

[8] The position of the IMAGE spacecraft at 0820 UT was (X_{GSM}, Y_{GSM}, Z_{GSM}) = (3.1 R_E, 1.2 R_E, 6.8 R_E) in the magnetosphere. A sphere of radius 8 R_E was used as a "screen" [e.g., *Taguchi et al.*, 2005] to monitor the source ions for the LENA cusp signal. We used LENA data from the FOV of 16 sectors covering the general direction of the high-altitude cusp while excluding the "Sun signal," which is produced primarily by the charge exchange of solar wind protons prior to the protons being slowed and heated across the bow shock [*Collier et al.*, 2001a, 2001b, 2003]. For mapping to the ionosphere (and Figure 3, shown later), we used the Tsyganenko 96 (T96) model with the inputs of (B_Y, B_Z) = (10, −5) nT, P_{dyn} = 8 nPa, and Dst = −38 nT.

[9] As shown by the timestamps for the DMSP passes (red and blue lines) in Figure 1, both spacecraft flew through the near-noon sector from the postnoon to prenoon sectors using similar trajectories. DMSP F12 (red line) crossed the 1200 MLT meridian only 50 s later than F14. The green and red triangles on the passes indicate the boundaries of the ion precipitation, which were determined from the ion spectrogram shown below in Figure 2.

[10] Figures 2a and 2b show particle measurements obtained from DMSP F14 and F12, respectively, as functions of UT, which include the intervals shown in Figure 1. The spectrogram shown in Figures 2a and 2b indicates the directional differential fluxes of the electrons and ions with energies between 30 eV and 30 keV. Both spacecraft initially measured regions in which the energy fluxes of electron precipitation were very low and the ion precipitation had relatively high energies (the so-called central plasma sheet). The DMSP F14 (Figure 2a) and DMSP F12 (Figure 2b) spacecraft entered the boundary plasma sheet at approximately 0815:20 UT and 0817:10 UT, respectively; here, the ions have energies as low as a few hundred eV, and the electrons have accelerated fluxes with peak energies between ∼1 keV and a few hundred eV. The high-latitude portion of the boundary plasma sheet appears to be smoothly connected to the low-latitude boundary layer, where the fluxes of the ions and electrons are much lower.

[11] Subsequent to the time indicated by the green triangle on the left, each spacecraft entered a region where the ion precipitation had energies of roughly 1 keV and relatively

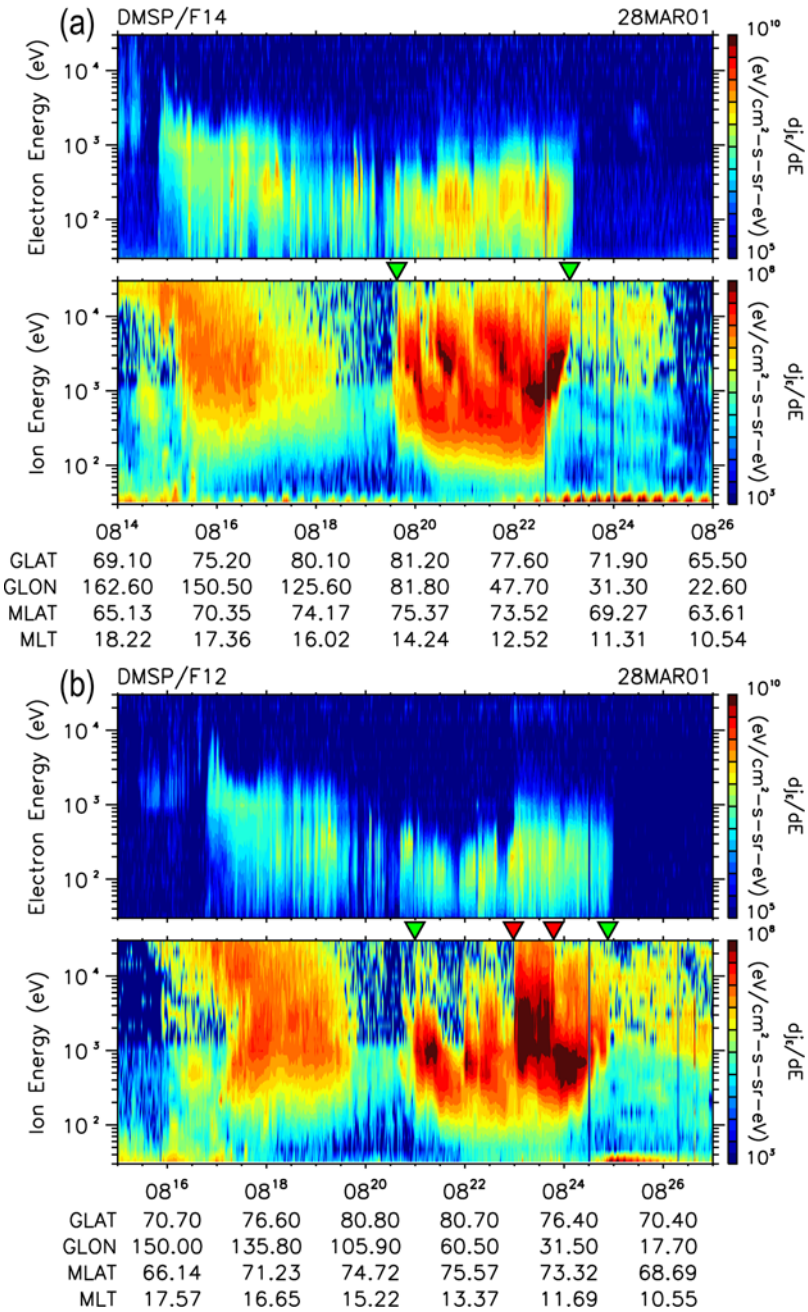

Figure 2. DMSP F12 and F14 measurements for electrons and ions on 28 March 2001. The green triangles indicate the interval of the cusp observation. The red triangles in the ion spectrogram of F12 show the ion precipitation burst, which is focused on in this study.

high fluxes. The spacecraft remained in this high-flux region until the time indicated by the green triangle on the right. The interval between the two green triangles can be defined as the cusp. For both passes, the latitude of the green triangles on the right is approximately 72° MLAT in the prenoon sector. In the postnoon sector, the two poleward boundaries of the cusp (indicated by the green triangles on the left) also lie at similar latitudes (~75°). The range 72°–75° is typical for the cusp of IMF with B_Z from −5 to −3 nT [*Newell et al.*, 1989]. The IMF data are shown later.

[12] For both passes, the cusp ion precipitation had multiple stepped structures. As expected, these structures are similar for both passes. The multiple stepped pattern for this event is different from the one reported in previous studies based on DMSP [e.g., *Newell and Meng* 1991; *Pinnock et al.*, 1995] and DE 2 observations [*Escoubet et al.*, 1992] in that the most equatorward portion did not have the highest average energy.

[13] In Figure 2b, the red triangles show the interval during which the ion precipitation had very large energy fluxes or the ion precipitation burst occurred. The energy flux at energies of ~700 eV to a few keV is particularly large, namely, ~1 × 10^8 eV cm^{-2} s^{-1} sr^{-1} eV^{-1}, and the total energy flux is as high as 1 × 10^{12} eV cm^{-2} s^{-1} sr^{-1}

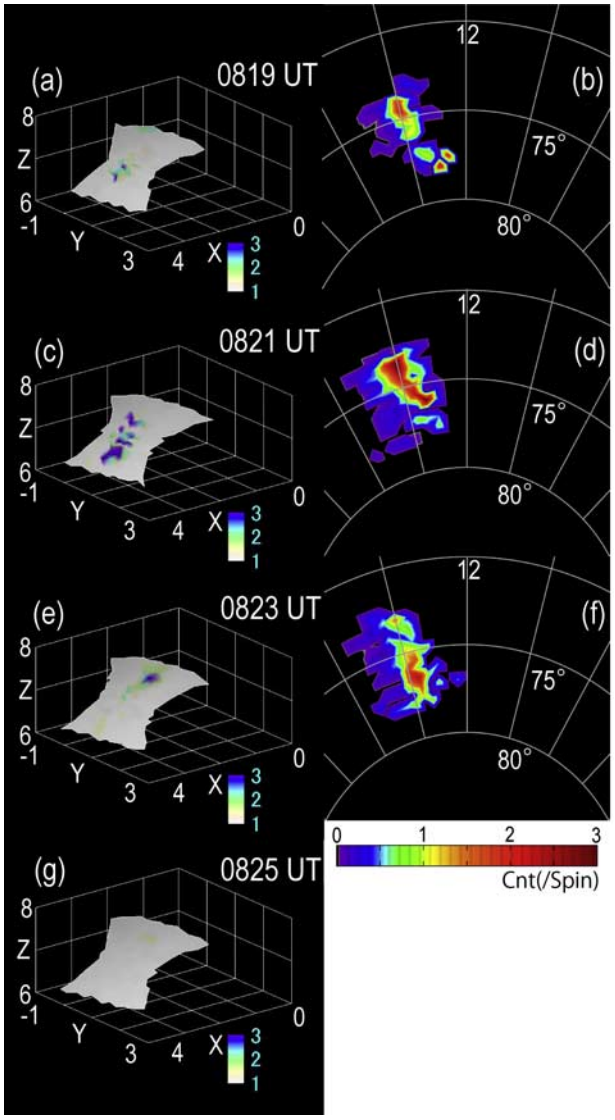

Figure 3. (left) LENA snapshots plotted on the sphere with a radius of 8 R_E and (right) their ionospheric projection. ENA signals were enhanced at 0821 UT. Ionospheric projection is not given for 0825 UT because no significant ENA signals were detected.

(not shown). The ions seem to have significant fluxes at energies above the upper limit of the sensor (30 keV). This type of intense precipitation was observed only by DMSP F12 and not by F14, although the general ion precipitation patterns observed by these spacecraft in the cusp are similar to a certain degree. F14 traversed the cusp at slightly lower latitudes and slightly before the traversal of F12; therefore, the fact that an ion burst was not observed indicates that the ion burst either occurred after the cusp crossing of F14 or was observable only on the poleward side of the F14 trajectory. We used LENA data to determine when the ion burst actually occurred.

[14] For more than 1 h, including the duration of the DMSP ion burst observations, LENA observed ENA signals from the high-altitude cusp. LENA responds to neutral atoms with energies from 10 eV up to at least 3–4 keV [*Moore et al.*, 2003]. ENAs are emitted by the charge exchange of ions with the hydrogen exosphere, and the flux of the ENAs detected by the instrument can be expressed as the line of sight (LOS) integration of the product of the source ion flux and the hydrogen exospheric density [e.g., *Roelof and Skinner*, 2000]. The ENAs essentially retain the energy and the direction of the incoming ions, and the detected ENA flux is proportional to the source ion flux.

[15] Figure 3 shows the LENA snapshots from the FOV looking into the general direction of the high-altitude cusp and the ionospheric projection of the snapshots. In the left column, the hydrogen count rate for each line of sight is plotted on the sphere with a radius of 8 R_E. The purple color represents the region with a relatively high count, which is defined as a count that is $\geq$3. The plots on the right are the ionospheric projections in which the LENA snapshots are mapped to an altitude of 110 km from the sphere with a radius of 8 R_E by using the T96 model.

[16] When we compared the ENA signals at 0819 UT (Figures 3a and 3b) and 0821 UT (Figures 3c and 3d), we noticed that the ENA emissions are enhanced at 0821 UT. This suggests that the flux of the injected ions increased at 0821 UT. Relatively high counts are mapped to latitudes higher than 73° MLAT (Figure 3d). This latitude is very close to that for the DMSP F12 observation of the ion burst. Under the assumption that the ion transit time from the high altitude to the low altitude is 2 min, the enhanced injection observed by LENA should appear in the ionosphere at around 0823 UT. This is in agreement with the DMSP F12 observations of the ion burst and is consistent with the fact that no ion burst was observed by F14 in a similar position approximately 1 min earlier.

[17] The LENA snapshot at 0823 UT (Figure 3e) shows that the injection region shifted somewhat poleward when compared to that at 0821 UT. A corresponding shift can be seen in Figure 3f, which indicates that the equatorward boundary of the relatively strong signals moved poleward by 1°–2° over a period of 2 min. Figure 3g (for 0825 UT) shows no significant signals within the FOV. This suggests that the ion injection within the FOV ceased or became so weak that the produced ENAs were not detectable. Since an intense ion injection is observed by DMSP F12 at 74°–75° MLAT near 1200 MLT, westward side of the LENA's FOV, it appears that the ion injection region with very large fluxes moved out of the LENA's FOV through the westward boundary of the FOV.

[18] Such westward motion and related features were observed by the SuperDARN radars, ESR, and the ground-based magnetometers of the IMAGE chain. Figure 4 shows the LOS velocity obtained from the SuperDARN radars (PYK and HAN), the field-aligned ion temperature obtained from ESR, and the Y component (eastward) of the perturbation to the geomagnetic field obtained by four ground-based magnetometers of the IMAGE chain at Ny Alesund (NAL), Longyearbyen (LYR), Hornsund (HOR), and Bear Island (BJN). Figure 4 also shows the ACE solar wind and the Polar magnetic field in the magnetosheath. For comparison with the ground station data, the ACE and Polar data were delayed by 40 and 4 min, respectively.

[19] Over the entire plotted interval, the solar wind speed is relatively constant at approximately 650 km s^{-1} (Figure 4a)

and the solar wind number density varies from 6 to 13 cm^{-3} (Figure 4b). Because of the enhanced density and the relatively high solar wind speed, the solar wind dynamic pressure (Figure 4c) is also relatively high (4–10 nPa). The dynamic pressure is calculated from the speed (Figure 4a) and density (Figure 4b) assuming the presence of 4% He^{++} particles.

[20] During this interval, the ACE IMF B_Y (blue in Figure 4d) was strongly positive and was the dominant component. The variations in the IMF B_Z component (red in Figure 4d) were mostly within ±7 nT. Figure 4e shows the magnetic field data obtained from the Polar spacecraft. The data at the beginning of the plotted interval corresponds to the magnetosphere; the Polar spacecraft exited the magnetosheath several minutes later. The Polar magnetic field variations in the sheath are correlated with the ACE magnetic field variations (Figure 4d). On the basis of this correlation, we chose 36 min (=40 min – 4 min) as the solar wind convection time from ACE to Polar.

[21] Figure 4f shows the data obtained from the SuperDARN PYK radar (beam 6). The LOS velocities around range gate 43 (indicated by the dashed line), corresponding to the LYR position, were directed toward the radar (bluish/greenish color); this shows that the flow had a westward component. The PYK data also indicate that the LOS velocities increased at around 0825 UT (indicated by an arrow), a few minutes after the time of the ion burst (red triangles), and that the LOS velocities reached 1.4 km s^{-1}. The HAN radar (Figure 4g) observed the appearance of LOS velocities toward the radar (greenish and bluish colors indicated by an arrow) concurrently with the flow enhancement observed by the PYK radar. The magnitude of the LOS velocities toward the HAN radar was approximately 500 m s^{-1}.

[22] Although the HAN radar is located in the near-noon sector (Figure 1), the LOS velocities toward the radar do not necessarily indicate sunward flow. If the flow has a strongly azimuthal component, some beams of the HAN radar would indicate LOS velocities toward the radar. For example, if we assume that the flow is parallel to beam 6 of the PYK radar, i.e., strongly westward above LYR, and that the flow magnitude is approximately 1.4 km s^{-1}, the velocities projected on beam 9 of the HAN radar would have a component toward the radar with a magnitude of approximately 500 m s^{-1} (=1.4 km s^{-1} × cos 70°).

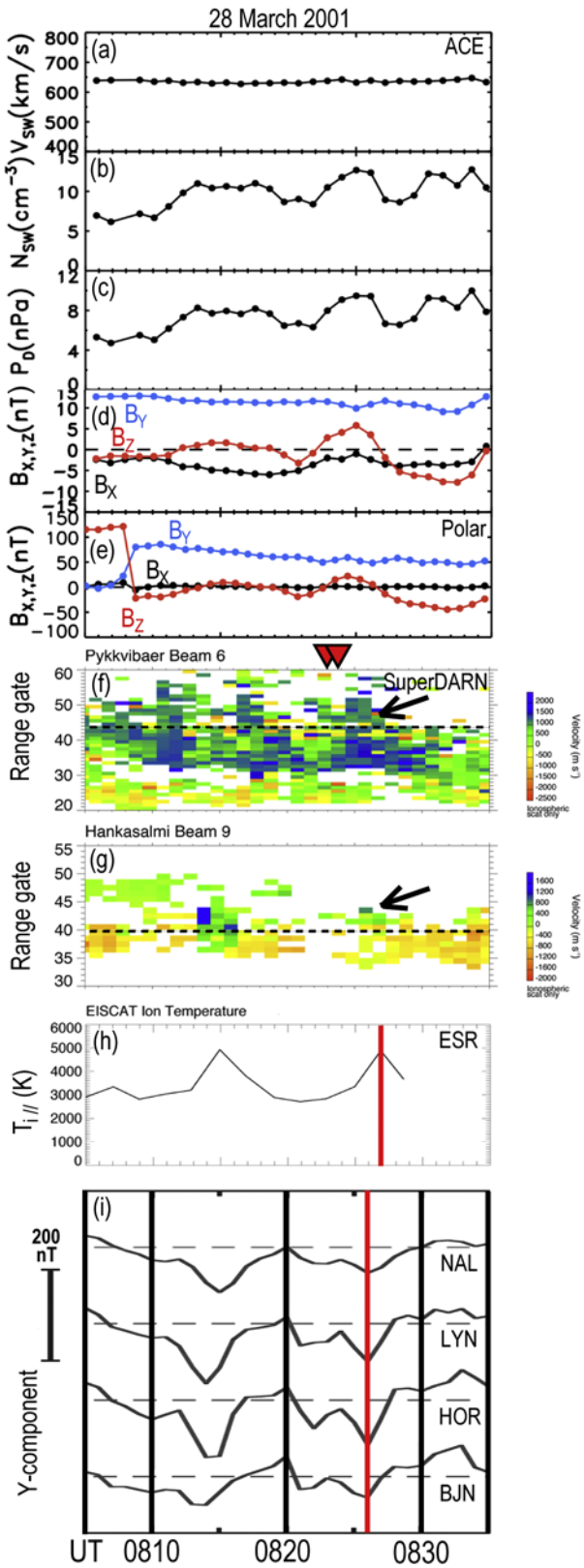

Figure 4. (a) Plasma velocity, (b) number density, (c) dynamic pressure, (d) three components of the interplanetary magnetic field in GSM coordinates, as seen by the ACE spacecraft in the solar wind, (e) three components of Polar magnetic field in GSM, (f) LOS velocity from the SuperDARN radar at Pykkvybaer, (g) that from Hankasalmi, (h) field-aligned ion temperature from ESR, and (i) Y component (eastward) of the perturbation to the geomagnetic field obtained by four ground-based magnetometers of the IMAGE magnetometer chain, NAL, LYR, HOR, and BJN. In Figure 4d, 64-s averages of IMF data that were created from original 16-s averages are plotted so as to make comparison between the IMF and plasma data easier. The ACE and Polar data are delayed by 40 and 4min, respectively. The dashed line in Figures 4f and 4g show the range gate corresponding to the ESR position. The vertical red lines in Figures 4h and 4j show the peak of the perturbation, which we focus on.

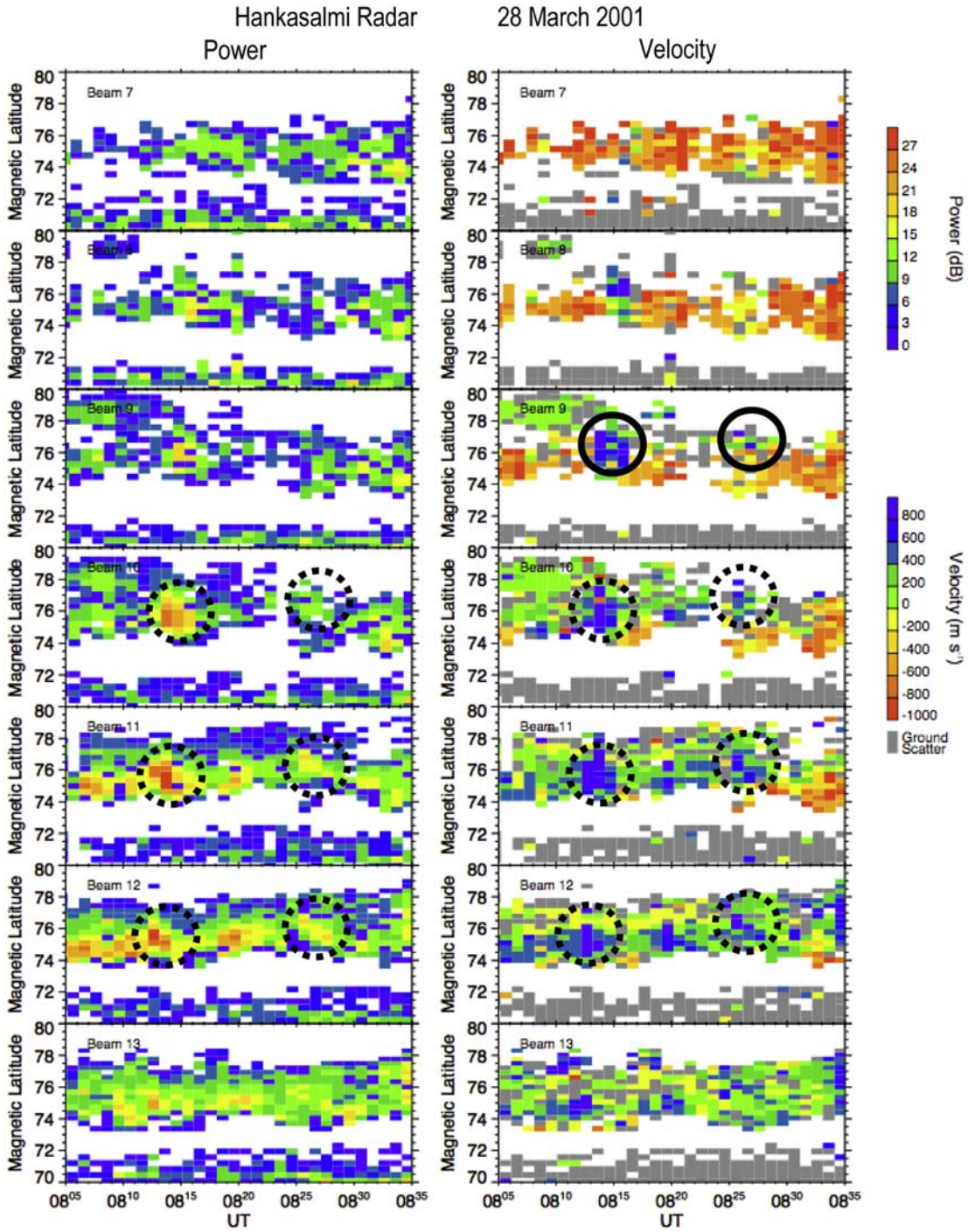

Figure 5. (left) Backscatter power and (right) line of sight velocity for beams 7 to 13 at the SuperDARN Hankasalmi radar. Two solid circles in the plot for the line of sight velocity from beam 9 indicate the flow enhancements, which have been identified in Figure 4. Dotted circles represent power and velocity enhancements in beams 10–12.

[23] In general, the velocity observed by the SuperDARN radar tends to be slightly smaller than the ion drift velocity observed by in situ spacecraft. *Drayton et al.* [2005] have shown that the slope of the best linear fit of the velocity observed by the PYK radar to that observed by the DMSP ion drift meter is approximately 0.6. The actual speed obtained from this ratio would be approximately 2.3 km s^{-1} (=1.4 km s^{-1}/0.6). As shown below, this speed is consistent with that estimated from the ESR observation.

[24] The ESR observation is shown in Figure 4h. Variations in the field-aligned ion temperature (2 min integrations) at a height of approximately 650 km show an enhancement that occurred concurrently with flow enhancements identified by the HAN radar (Figure 4g). The temperature increases

up to ~1700 K relative to the background level of ~3000 K both at 0815 and 0827 UT (indicated by the red line).

[25] When an ambient gas is assumed to consist of atomic oxygen, the ion temperature, T_i due to the frictional heating can be expressed in MKS units as

$$T_i = T_n + 6.5 \times 10^{-4} |\boldsymbol{V}_i - \boldsymbol{V}_n|^2, \quad (1)$$

where $\boldsymbol{V}_i$ and $\boldsymbol{V}_n$ are the ion and neutral gas velocity, respectively, and T_n represents the neutral gas temperature [e.g., *Schunk et al.*, 1975]. Taking into consideration the increase in the flow and the consequent increase in ion temperature, ΔT_i, equation (1) can be written as

$$|\boldsymbol{V}_{iE} - \boldsymbol{V}_n|^2 = 1.5 \times 10^3 (T_i + \Delta T_i - T_n), \quad (2)$$

where $\boldsymbol{V}_{iE}$ is the enhanced ion velocity. Then the following rough inequality is obtained for the enhanced ion velocity when $\boldsymbol{V}_{iE} // \boldsymbol{V}_n$ is assumed:

$$|\boldsymbol{V}_{iE}| > |\boldsymbol{V}_n| + 40(\Delta T_i)^{1/2}. \quad (3)$$

[26] For a ΔT_i ($\sim \Delta T_{i\|}$) of 1700 K (shown in Figure 4h), $|\boldsymbol{V}_{iE}|$ is estimated to be greater than 2.1×10^3 m s^{-1} when 500 m s^{-1} is taken as a typical value of $|\boldsymbol{V}_n|$ [e.g., *Hays et al.*, 1984]. This speed is consistent with the flow speed estimated from the SuperDARN radar (2.3 km s^{-1}). We note that this speed is also very close to that of the moving proton aurora spot (2.4 km s^{-1}) reported by *Suzuki et al.* [2008].

[27] The magnetometer data from four stations (Figure 4i) also support the occurrence of enhancements of the westward flow. A clear negative perturbation in the *Y* component occurs almost at the same time as when the field-aligned ion temperature measured by ESR reaches a peak. From the theorem by *Fukushima* [1969], the magnetic field of the Pedersen current is canceled by that of the field-aligned current. The magnetic perturbation must be explained by the Hall current.

[28] A negative perturbation in the *Y* component indicates that the Hall current has a component toward the North Pole (Figure 1); in other words, the flow must have a southward component in the geographic coordinates. This is seemingly contradictory to the observation that the flow is enhanced in the westward direction. However, if the westward flow only has to be aligned with the azimuthal direction in the MLAT-MLT coordinates, it can have a southward component in the geographic coordinates (map in Figure 1); this explains a negative magnetic perturbation in the *Y* component.

[29] How the enhanced westward flow region moves can be seen in data from several beams of the HAN radar. In Figure 5, we show the backscatter power and LOS velocity data from beams 7 (top) to 13 (bottom) as functions of UT and magnetic latitude. Radar beams labeled with higher numbers are directed toward the further eastward portion of the FOV. For example, beam 13 crosses the noon meridian (12 MLT) at 74° MLAT, which is 1 h in MLT away from LYR.

[30] In the third row (beam 9) in Figure 5 (right), the data used in Figure 4g are plotted on a different unit of the vertical axis. The two solid circles (~0815 and ~0826 UT) represent the enhancement of the westward flow mentioned above. The dotted circles represent the power and flow enhancements observed in beams 10–12. For the first event, the enhancement started at 0812 UT in beams 11–12 and arrived at the region just westward of LYR, which is covered by beam 8. The backscatter power data (left column) show that the enhanced power features are associated with the velocity enhancement. For the second event, which is the main event discussed in this paper, a similar isolated enhancement can be observed although its motion is not clearly identified. The enhancement both in the LOS velocity and in backscatter power was observed at 0825–0827 UT (beams 10–12), 1–3 min after the DMSP observation of the ion burst.

[31] Beams 9 and 12 cross the ~1100 MLT and ~1145 MLT meridians at 75° MLAT. The simultaneous observation of the flow enhancement in beams 9–12 indicates that the longitudinal range of the flow enhancement is approximately 350 km. This observation is discussed later. We note that the maximum backscatter power of beam 12 shifts toward lower latitudes at around 0826 UT. This observation will be incorporated in the interpretation presented later.

[32] Figure 6 shows 1-min integrations of the ESR data in the interval from 0800 to 0830 UT. The data on electron density, electron temperature, field-aligned ion temperature, and field-aligned ion velocity are plotted as functions of altitude and time. The electron-density data (Figure 6a) show that an enhancement occurs at 0826 UT. The electron temperature (shown in Figure 6b) is also increased at this time, and these facts suggest that the electron precipitation becomes strong above ESR at 0826 UT. This indicates that the enhanced westward flow above ESR is accompanied by intense plasma precipitation. A similar correspondence can be identified at ~0815 UT, suggesting that the same process occurs at ~0815 and ~0826 UT. Figure 6c shows that the ion temperature increases at 0815 and 0826 UT, as was shown in Figure 4h. The upward flow is enhanced at the same time as the increase of the electron density/temperature, and of the ion temperature (Figure 6d).

3. Interpretation and Discussion

3.1. Moving Mesoscale Plasma Precipitation

[33] The abovementioned enhancement of the westward flow explains the 3-min (0826 UT–0823 UT) delay in the ground magnetic field perturbation at ~1100 MLT from the ion burst detected at ~1200 MLT. Since the magnetic perturbations at ~1100 MLT were larger at LYR and HOR than at NAL and BJN, the center latitude of the enhanced convection was close to LYR and HOR (74°–75° MLAT). These latitudes are just ~1° poleward of the latitude at which the ion burst was observed. The distance from the location of the ion burst observation (74°–75° MLAT at ~1200 MLT) to the location above LYR and HOR (74°–75° MLAT at ~1100 MLT) is approximately 450 km. The delay of 3 min can be attributed to the flow speed of 2.3 km s^{-1} because the transit time would be approximately 3 min (=450 km/2.3 km).

[34] As shown in Figures 4h and 4i, the duration of the flow enhancement (or ground magnetic perturbation) was 2–3 min. From this duration and the estimated flow speed of 2.3 km s^{-1}, we can estimate the scale of the flow

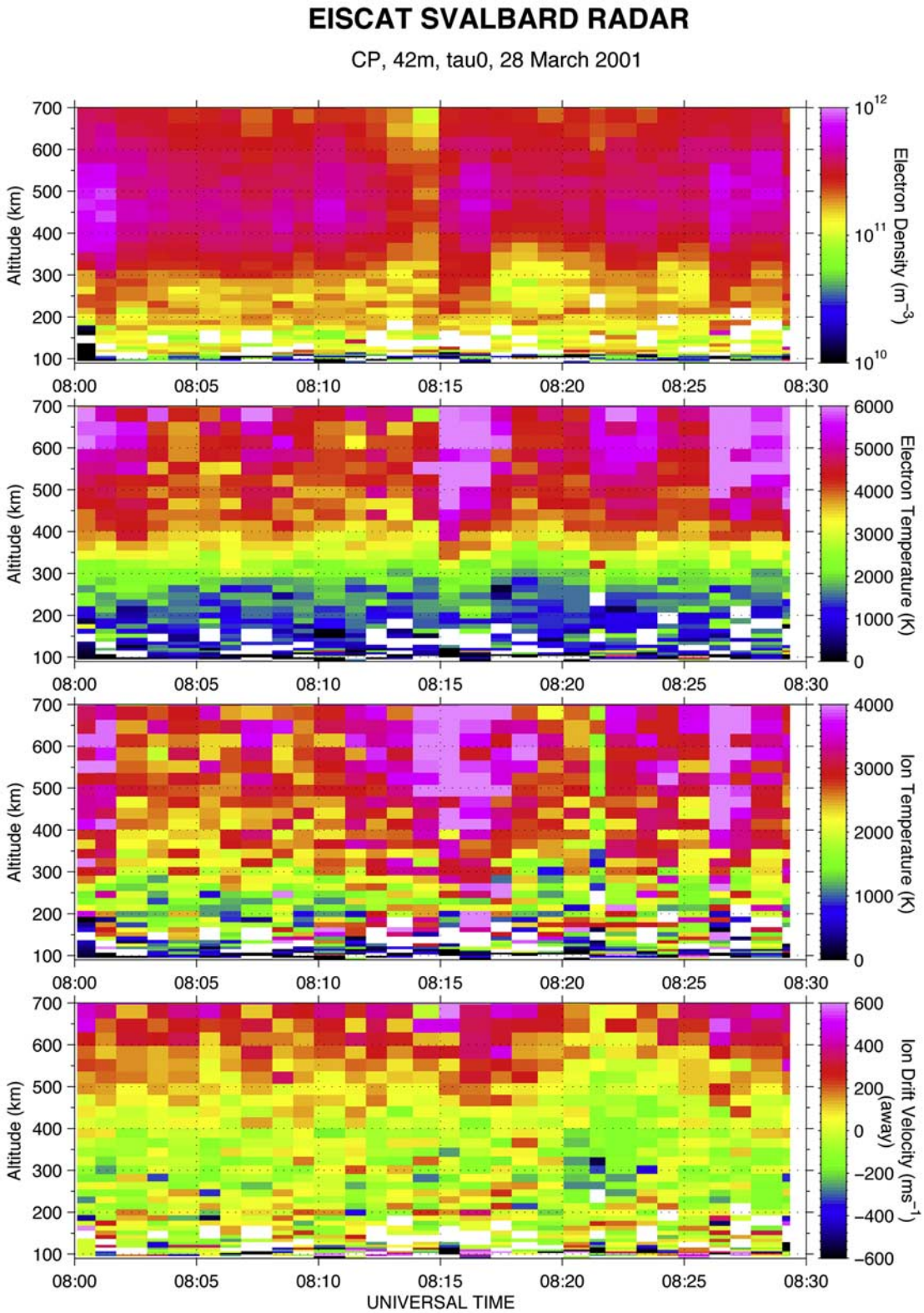

Figure 6. One-minute integrations of the data from the field-aligned ESR beam for the interval of 0800-0830 UT. (a, b) Electron density and temperature. (c) Field-aligned ion temperature and (d) field-aligned ion velocity.

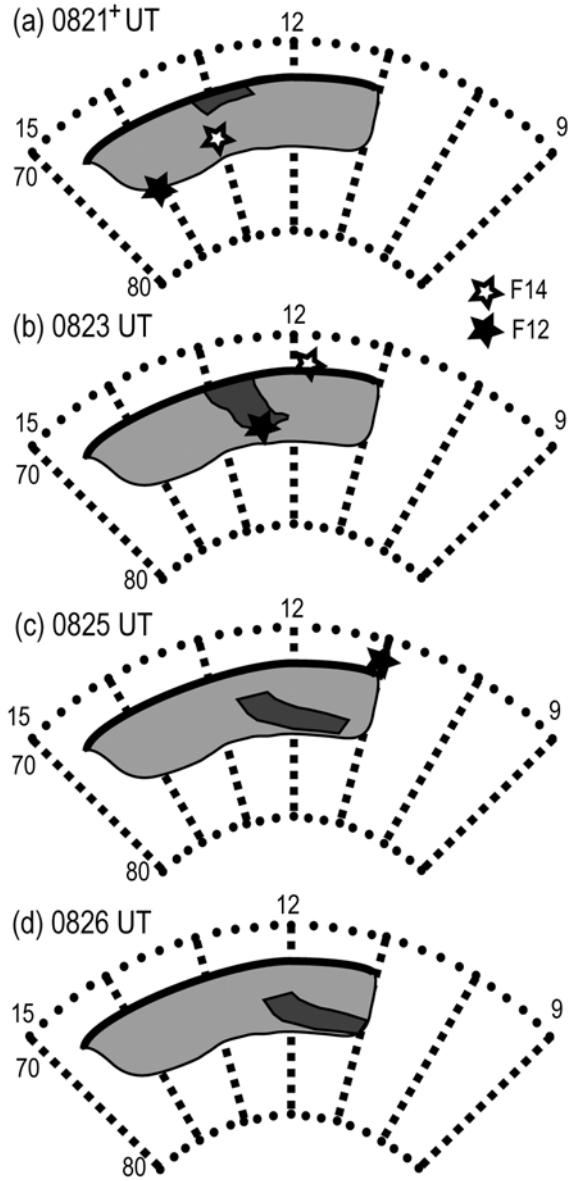

Figure 7. Schematic illustration of the time sequence for the moving mesoscale plasma precipitation, shown in the MLAT-MLT coordinate.

enhancement region in the direction of motion to be 300–400 km. This scale is in agreement with the longitudinal range obtained from the SuperDARN data shown in Figure 5.

[35] Figure 7 shows a schematic illustration of our interpretation of the time sequence for the enhanced westward flow in the mesoscale ion precipitation region. Hereinafter, we refer to this region as the moving mesoscale plasma precipitation (MMPP). The dark-gray-colored region in each map in Figure 7 represents the MMPP. From a part of the footprint of the reconnection line (bold curve at ~72° MLAT), MMPP appeared together with enhanced flow.

[36] We draw the reconnection line between 1100 and 1430 MLT (3.5 h) simply on the basis of the MLT of the cusp crossing (green triangles in Figure 1). The light gray region extending poleward from the reconnection line represents the cusp where the ion precipitation occurred. The poleward boundary of this region is shown to be at ~75° MLAT, which reflects the position of the green triangles on the left in Figures 1 and 2. Since the two DMSP passes exited the cusp at 1100 MLT or later, we do not know how the cusp extended to the earlier MLT. However, the 3.5-h width of the cusp may be representative of a situation for this relatively high dynamic pressure because this width agrees with the statistical results of *Newell and Meng* [1994] for high dynamic pressure.

[37] In Figure 7a, an illustration of the situation just after the appearance of the MMPP is shown. The ion injection burst in this situation was not detected by LENA at the high altitude. We do not have direct evidence that shows exactly when the ion burst started. However, since the DMSP observation of the ion burst at 74°–75° MLAT at ~1200 MLT is 0823 UT, and a plausible transit time to this site from the footprint of the reconnection line, for a speed of 2–3 km s^{-1}, is approximately 2 min, the ion burst must have appeared at the ionospheric height immediately after 0821 UT (shown as 0821^+ UT in Figure 7a.) In Figure 7a, the two star marks indicate the location of DMSP F12 and F14 at around 0821 UT. At this time, the MMPP was located away from the spacecraft.

[38] At 0823 UT (Figure 7b), F14 reached the equatorward edge of the cusp without traversing the MMPP, while F12 observed the MMPP, which had just extended from the eastward side of F12. Figure 7b also depicts the situation when the ion injection burst was detected by LENA. Since the equatorward boundary of the relatively strong ENA signals is mapped to ~73° MLAT (Figure 3d), which is very close to the equatorward boundary of the cusp, the MMPP would still be connected to the reconnection line. We draw the reconnection line for the MMPP at this time in somewhat earlier MLT than that for 0821 UT^+. The westward flow emerging from such a reconnection line tends to pass through lower latitudes. This may explain the shift in the maximum backscatter power toward lower latitudes (Figure 5).

[39] The center latitude of the MMPP at noon was roughly 75°. This appears to be the typical latitude at which the flow speed, i.e., electric field, or the equivalent magnetic perturbation caused by the field-aligned current for the cusp shows a maximum during the $|B_Y| \gg |B_Z|$ condition [*Taguchi et al.*, 1993]. As estimated above, the horizontal size of the MMPP in the flow direction is roughly 350 km. As shown in the F12 observation, the MMPP was detected in a latitudinally narrow (approximately 100-km wide) region. These suggest that the MMPP has a longitudinally elongated form. During the interval of this event, FUV/IMAGE did not provide proton aurora data. However, if FUV/IMAGE was in operation, the moving proton aurora spot would have been observed as reported by *Suzuki et al.* [2008].

[40] The illustration in Figure 7c shows the situation at 0825 UT, which corresponds to the LENA observation at 0823 UT (Figures 3e and 3f). As suggested by the motion of the LENA signals, the MMPP was no longer connected to the reconnection line. The leading edge of the MMPP approached the location of LYR. This is inferred from the SuperDARN radar and ground magnetometer data. The SuperDARN observed flow enhancements at this time (Figure 4f), and the ground magnetometer detected the start

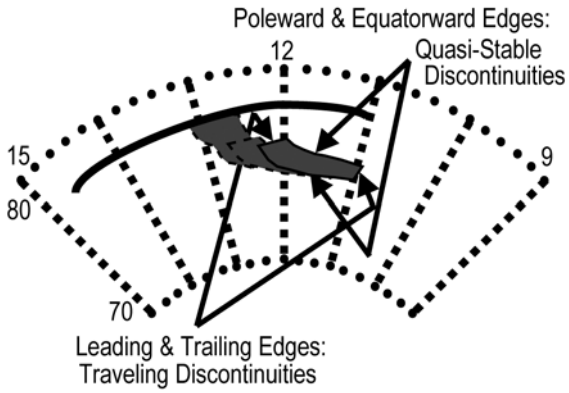

Figure 8. Relation of MMPP to the temporal and spatial structures of the cusp.

of the magnetic field perturbation (Figure 4i). The trailing edge would be located at 1230–1300 MLT because the ENA emissions were still in LENA's FOV (Figure 3e).

[41] Figure 7d shows the situation after 1 min. At this time, LYR and HOR were within the MMPP, and the enhanced Hall current in the MMPP produced the magnetic perturbations with a negative *Y* component (Figure 4i). As suggested by the ESR data, the plasma precipitation still occurred at this stage (~5 min after the appearance of the MMPP). This is consistent with the duration (4–6 min) of the moving proton aurora spot reported by *Suzuki et al.* [2008].

3.2. Temporal and Spatial Structures of the Cusp

[42] In Figure 8 we show how the MMPP is related to the temporal and spatial structures of the cusp. Since the particle injection in the cusp is caused by reconnection, the leading and trailing edges of the MMPP should be created by the temporal effect of the reconnection. The decrease in the reconnection rate leads to the creation of the trailing edge; in other words, the MMPP is detached from the reconnection line. These edges move in the direction of the flow, and appear as traveling discontinuities within the cusp. The other edges of the MMPP, which lie along the streamline, are the equatorward and poleward boundaries of the MMPP during the majority of this period. These edges originate in a spatially limited region along the reconnection line. The MMPP has a form whose boundary is delineated by both the temporal and spatial structures of the cusp. The latitude at which the poleward/equatorward edge appears is almost constant during a certain period of time because the longitudinally elongated structure moves in the longitudinal direction. In this sense, these edges are quasi-stable discontinuities within the cusp.

[43] Spatial cusp structures are thought to be the result of multiple reconnection lines [e.g., *Weiss et al.*, 1995; *Wing et al.*, 2001, *Trattner et al.*, 2002, 2005]. In the present event, the MMPP appeared as a mesoscale structure inside the larger region of the cusp. Whether the MMPP and the cusp region outside the MMPP originated from separate reconnection lines is not determined in this study. In Figure 8 (also Figure 7), we have considered a single reconnection line for simplicity (bold curve). Such a single reconnection line may be possible if the temporal variation in the reconnection rate is different along the line.

3.3. Relation of the MMPP to Previous Studies

[44] The above interpretation is valid for several previous observations. If a low-altitude spacecraft enters or exits the cusp through the equatorward boundary of the MMPP in the situation depicted in Figure 7a or 7b, the satellite would observe features in which the ion burst appears in the most equatorward part of the cusp. This explains the observation that the ion bursts occur in spatially discrete regions on the equatorward edge of the cusp [*Newell and Meng*, 1991].

[45] In this event, no clear dispersion was observed inside the MMPP. Figures 7a and 7b suggest that the DMSP F12 pass during the MMPP was roughly parallel to the reconnection line from which the MMPP originated. The precipitating ions along the pass inside the MMPP would have a similar transit time from the reconnection line; therefore, no clear dispersion may be observed. If the pass is more meridional, the satellite will observe the clear dispersion in which the average energy decreases with an increase in latitude. On the other hand, if the satellite passes more longitudinally through the MMPP, a reversed dispersion, which is usually observed for lobe reconnections typical for northward IMF [e.g., *Burch et al.*, 1980], would be observed. Caution must be exercised in interpreting the reversed dispersion observed along the longitudinal pass in terms of the lobe reconnection.

[46] Using particle data from the meridional pass of DE 2 at ~1000 MLT, *Escoubet et al.* [1992] reported three distinct ion populations whose peak flux energy decreases with an increase in latitude. They interpreted these ion steps as three consecutive flux transfer events (FTEs). In the framework of our interpretation, these three regions can be created by the three MMPPs originating in different, adjacent MLT regions and then moving in a similar manner in the azimuthal direction.

[47] The longitudinally elongated form of the MMPP appears to be similar to the midday auroral breakup event identified in the cusp from the ground-based optical observations made by *Sandholt et al.* [1989]. *Sandholt et al.* [1989] have shown that this aurora often exhibits large longitudinal motion, and that the duration of motion is typically between 5 and 10 min, which is consistent with our interpretation. *Fasel et al.* [1993] referred to this type of aurora as the poleward-moving auroral form (PMAF), and since then, PMAF has been widely accepted as the typical transient auroral signature in the cusp.

[48] Although the PMAF and MMPP share some common features, we do not refer to the present event as PMAF for the following reasons. Firstly, the PMAF is produced by the electron precipitation, but for our event, intense ion precipitation is prominent. Secondly, the deduced motion of the MMPP is westward and the poleward component is very small, which was in fact reported earlier by *Sandholt et al.* [1989]; hence the use of the term PMAF might lead to misinterpretation. Finally, we would like to emphasize the importance of the mesoscale structure of the plasma precipitation rather than the direction of motion, which reflects the characteristics of the dayside reconnection.

[49] We have shown that the MMPP can exist as a detached structure from the reconnection line; i.e., a few

degrees poleward from the line. This indicates that the ion injection still occurs along the flux tubes away from the reconnection point, presumably at high latitudes on the dayside magnetopause. Using high-latitude magnetic field data from the HEOS-2 spacecraft, *Haerendel et al.* [1978] identified signatures showing the transient nature of the reconnection. *Wild et al.* [2001] observed FTE at the high-latitude magnetopause using data from the Cluster spacecraft and inferred that the FTEs travel for a few minutes after a reconnection burst. This kind of high-latitude FTE would be the magnetospheric counterpart of the MMPP.

[50] Several studies have shown that the FTE is responsible for the convection flow burst in the ionosphere. This has been shown, for example, by *Lockwood et al.* [1990], who utilized the ESR data. By using data from the HF radar at Hallery, Antarctica, *Pinnock et al.* [1991, 1993] and *Rodger et al.* [1994] showed that the flow burst can be longitudinally elongated (by at least 900 km) and attributed the burst to a patchy reconnection. In the present event, we estimate the duration of the reconnection enhancement to be approximately 3 min. If the reconnection enhancement continued, a more elongated region would have formed, as shown by *Pinnock et al.* [1991, 1993] and *Rodger et al.* [1994]. *Wild et al.* [2001] also reported that multiple poleward-moving enhancements were observed in the backscatter echoes of the SuperDARN radar during intervals when many FTEs were observed in the magnetopause, although the clearest signatures in the ionosphere are displaced by ~2 MLT from the Cluster footprint.

4. Conclusions

[51] We presented a study on an event that occurred on 28 March 2001, when the IMF was strongly duskward. This study is based on simultaneous observations of the ENA cusp signals obtained from LENA on the IMAGE spacecraft, the ion precipitation burst observed by the DMSP F12 spacecraft, the ion drift observed by the SuperDARN radar, the plasma temperature and concentration obtained from ESR, and the ground magnetic perturbation in the IMAGE magnetometer chain. These observations cover a longitudinally wide region of the cusp, and strongly suggest the existence of a mesoscale plasma precipitation moving with an enhanced flow in the longitudinal direction. The moving speed is estimated to be approximately 2.3 km s^{-1}. The precipitation region has a longitudinal scale size of 300–400 km and a latitudinal scale size of ~100 km, i.e., a longitudinally elongated form. The leading and trailing edges of this form should be created by the temporal change in the reconnection rate. The other edges appear as equatorward and poleward edges during most of the period and originate in a spatially limited region along the footprint of the reconnection line. The moving mesoscale plasma precipitation has a form whose boundary is delineated by both the temporal and spatial structures of the cusp.

[52] **Acknowledgments.** This research was supported by Grant-in-Aid for Scientific Research (C) 18540443 under Japan Society for the Promotion of Science, by National Institute of Polar Research collaboration project 20-7, and by the IMAGE Project under UPN 370-28-20 at Goddard Space Flight Center. The DMSP particle detectors were designed by David Hardy of AFRL, and data were obtained from JHU/APL. We thank David Hardy, Fred Rich, and Patrick Newell for its use. We also thank the institutes, which maintained the IMAGE magnetometers array. The IMEGE magnetometer data were collected as a Finnish-German-Norwegian-Polish-Russian-Swedish project. EISCAT is an international association, supported by research organizations in China, Finland, France (until 2006), Germany, Japan, Norway, Sweden, and the United Kingdom. CUTLUSS (Hankasalmi and Pykkvybaer radar pair) is supported by an award from STFC. The authors also thank C. T. Russell (PI of Polar magnetic field data), D. McComas (PI of ACE plasma data), and N. Ness (PI of ACE magnetic field data) for providing data through the NASA CDAWeb.

[53] Amitava Bhattacharjee thanks Alexandre Koustov and another reviewer for their assistance in evaluating this paper.

References

Burch, J., P. Reiff, R. Spiro, R. Heelis, and S. Fields (1980), Cusp region particle precipitation and ion convection for northward interplanetary magnetic field, *Geophys. Res. Lett.*, *7*(5), 393–396.

Collier, M. R., et al. (2001a), Observations of neutral atoms from the solar wind, *J. Geophys. Res.*, *106*(A11), 24,893–24,906.

Collier, M. R., et al. (2001b), LENA observations on March 31, 2001: Magnetosheath remote sensing, *Eos Trans. AGU*, *82*(47), Fall Meeting Suppl., Abstract SM41C-05, F1071-F1072.

Collier, M. R., et al. (2003), Dust in the wind: The dust geometric cross section at 1 AU based on neutral solar wind observations, in *Solar Wind Ten*, *Proc. of the Tenth Int. Solar Wind Conf.*, *AIP Conf. Proc.*, vol. 679, edited by M. Velli, R. Bruno, and F. Malara, pp. 790–793, American Institute of Physics, Melville, New York.

Collier, M. R., T. E. Moore, M.-C. Fok, B. Pilkerton, S. Boardsen, and H. Khan (2005), Low-energy neutral atom signatures of magnetopause motion in response to southward Bz, *J. Geophys. Res.*, *110*, A02102, doi:10.1029/2004JA010626.

Cowley, S. W. H., M. P. Freeman, M. Lockwood, and M. F. Smith (1991), The ionospheric signature of flux transfer events, in *CLUSTER: Dayside Polar Cusp*, *ESA, SP-330*, vol. 105, edited by C. I. Barron, Eur. Space Agency, Paris, France.

Drayton, R. A., A. V. Koustov, M. R. Hairston, and J.-P. Villain (2005), Comparison of DMSP cross-track ion drifts and SuperDARN line-of-sight velocities, *Ann. Geophys.*, *23*, 2479–2486.

Escoubet, C. P., M. F. Smith, S. F. Fung, P. C. Anderson, R. A. Hoffman, E. M. Basinska, and J. M. Bosqued (1992), Staircase ion signature in the polar cusp: A case study, *Geophys. Res. Lett.*, *19*(17), 1735–1738.

Fasel, G. J., L. C. Lee, and R. W. Smith (1993), A mechanism for the multiple brightenings of dayside poleward-moving auroral forms, *Geophys. Res. Lett.*, *20*(20), 2247–2250.

Fok, M.-C., et al. (2003), Global ENA IMAGE simulations, *Space Sci. Rev.*, *109*, 77–103.

Fukushima, N. (1969), Equivalence in ground geomagnetic effect of Chapman-Vestine's and Birkland-Alfven's electric current-systems for Polar magnetic storms, *Rep. Ionos. Space Res. Jpn.*, *23*(3), 219–227.

Greenwald, R. A., et al. (1995), DARN/SuperDARN: A global view of the dynamics of high-latitude convection, *Space Sci. Rev.*, *71*, 761–796.

Haerendel, G., G. Paschmann, N. Sckopke, H. Rosenbauer, and P. C. Hedgecock (1978), The frontside boundary layer of the magnetosphere and the problem of reconnection, *J. Geophys. Res.*, *83*(A7), 3195–3216.

Hays, P., et al. (1984), Observations of the dynamics of the polar thermosphere, *J. Geophys. Res.*, *89*(A7), 5597–5612.

Hosokawa, K., S. Taguchi, S. Suzuki, M. R. Collier, T. E. Moore, and M. F. Thomsen (2008), Estimation of magnetopause motion from low-energy neutral atom emission, *J. Geophys. Res.*, *113*, A10205, doi:10.1029/2008JA013124.

Lockwood, M., and M. F. Smith (1992), The variation of reconnection rate at the dayside magnetopause and cusp ion precipitation, *J. Geophys. Res.*, *97*(A10), 14,841–14,847.

Lockwood, M., S. W. H. Cowley, P. E. Sandholt, and R. P. Lepping (1990), The ionospheric signatures of flux transfer events and solar wind dynamic pressure changes, *J. Geophys. Res.*, *95*(A10), 17,113–17,135.

Mende, S. B., et al. (2000), Far Ultraviolet imaging from the IMAGE spacecraft, *Space Sci. Rev.*, *91*, 243–270.

Menietti, J. D., and J. L. Burch (1988), Spatial extent of the plasma injection region in the cusp-magnetosheath interface, *J. Geophys. Res.*, *93*(A1), 105–113.

Moore, T. E., et al. (2000), The low-energy neutral atom imager for IMAGE, *Space Sci. Rev.*, *91*(1-2), 155–195.

Moore, T. E., et al. (2001), Low Energy Neutral Atoms in the magnetosphere, *Geophys. Res. Lett.*, *28*(6), 1143–1146.

Moore, T. E., et al. (2003), Heliosphere-geosphere interactions using Low Energy Neutral Atom imaging, *Space Sci. Rev.*, *109*, 351–371.

Murata, Y., S. Taguchi, K. Hosokawa, A. Nakao, M. R. Collier, T. E. Moore, N. Sato, H. Yamagishi, and A. S. Yukimatu (2007), Correlative variations of the neutral atom emission in the high-altitude cusp and the low-altitude cusp, *J. Geophys. Res.*, *112*, A11208, doi:10.1029/2007JA012404.

Newell, P., and C.-I. Meng (1991), Ion acceleration at the equatorward edge of the cusp: Low altitude observations of patchy merging, *Geophys. Res. Lett.*, *18*(10), 1829–1832.

Newell, P. T., and C.-I. Meng (1994), Ionospheric projection of the magnetospheric regions under low and high solar wind pressure conditions, *J. Geophys. Res.*, *99*(A1), 273–286.

Newell, P. T., C.-I. Meng, D. G. Sibeck, and R. P. Lepping (1989), Some low-altitude cusp dependencies on interplanetary magnetic field, *J. Geophys. Res.*, *94*(A7), 8921–8927.

Nosé, M., S. Taguchi, K. Hosokawa, S. P. Christon, R. W. McEntire, T. E. Moore, and M. R. Collier (2005), Overwhelming O^+ contribution to the plasma sheet energy density during the October 2003 superstorm: Geotail/EPIC and IMAGE/LENA observations, *J. Geophys. Res.*, *110*, A09S24, doi:10.1029/2004JA010930.

Onsager, T. G., S.-W. Chang, J. D. Perez, J. B. Austin, and L. X. Janoo (1995), Low-altitude observations and modeling of quasi-steady magnetopause reconnection, *J. Geophys. Res.*, *100*(A7), 11,831–11,843.

Pinnock, M., A. S. Rodger, J. D. Dudeney, R. A. Greenwald, K. B. Baker, and J. M. Ruohoniemi (1991), An ionospheric signature of possible enhanced magnetic field merging on the dayside magnetopause, *J. Atmos. Terr. Phys.*, *53*, 201–212.

Pinnock, M., A. S. Rodger, J. R. Dudeney, K. B. Baker, P. T. Newell, R. A. Greenwald, and M. E. Greenspan (1993), Observations of an enhanced convection channel in the cusp ionosphere, *J. Geophys. Res.*, *98*(A3), 3767–3776.

Pinnock, M., A. S. Rodger, J. R. Dudeney, F. Rich, and K. B. Baker (1995), High spatial and temporal resolution observations of the ionospheric cusp, *Ann. Geophys.*, *13*, 919–925.

Reiff, P. H., T. W. Hill, and J. L. Burch (1977), Solar wind plasma injection at the dayside magnetospheric cusp, *J. Geophys. Res.*, *82*(4), 479–491.

Roelof, E. C., and A. J. Skinner (2000), Extraction of ion distributions from magnetospheric ENA and EUV images, *Space Sci. Rev.*, *91*, 437–459.

Rodger, A. S., M. Pinnock, J. R. Dudeney, K. B. Baker, and R. A. Greenwald (1994), A new mechanism for polar patch formation, *J. Geophys. Res.*, *99*(A4), 6425–6436.

Sandholt, P. E., B. Lybekk, A. Egeland, R. Nakamura, and T. Oguti (1989), Midday auroral breakup, *J. Geomagn. Geoelectr.*, *41*, 371–387.

Schunk, R. W., W. J. Raitt, and P. M. Banks (1975), Effect of electric fields on the daytime high-latitude E and F regions, *J. Geophys. Res.*, *80*(22), 3121–3130.

Suzuki, S., S. Taguchi, K. Hosokawa, M. R. Collier, T. E. Moore, H. U. Frey, and S. B. Mende (2008), Conjugate observations of ENA signals in the high-altitude cusp and proton auroral spot in the low-altitude cusp with IMAGE spacecraft, *Geophys. Res. Lett.*, *35*, L13103, doi:10.1029/2008GL034543.

Syrjaasuo, M., et al. (1998), Observations of substorm electrodynamics using the MIRACLE network, Substorms-4, by S. Kokubun and Y. Kamide, pp. 111–114, Terra Sci., Tokyo.

Taguchi, S., M. Sugiura, J. D. Winningham, and J. A. Slavin (1993), Characterization of the IMF BY-dependent field-aligned currents in the cleft region based on DE 2 observations, *J. Geophys. Res.*, *98*(A2), 1393–1407.

Taguchi, S., M. R. Collier, T. E. Moore, M.-C. Fok, and H. J. Singer (2004), Response of neutral atom emissions in the low- and high-latitude magnetosheath direction to the magnetopause motion under extreme solar wind conditions, *J. Geophys. Res.*, *109*, A04208, doi:10.1029/2003JA010147.

Taguchi, S., S.-H. Chen, M. R. Collier, T. E. Moore, M.-C. Fok, K. Hosokawa, and A. Nakao (2005), Monitoring the high-altitude cusp with the Low Energy Neutral Atom imager: Simultaneous observations from IMAGE and polar, *J. Geophys. Res.*, *110*, A12204, doi:10.1029/2005JA011075.

Taguchi, S., K. Hosokawa, A. Nakao, M. R. Collier, T. E. Moore, A. Yamazaki, N. Sato, and A. S. Yukimatu (2006), Neutral atom emission in the direction of the high-latitude magnetopause for northward IMF: Simultaneous observations from IMAGE spacecraft and SuperDARN radar, *Geophys. Res. Lett.*, *33*, L03101, doi:10.1029/2005GL025020.

Taguchi, S., K. Hosokawa, A. Nakao, M. R. Collier, T. E. Moore, N. Sato, and and A. S. Yukimatu (2009), HF radar polar patch and its relation with the cusp during BY-dominated IMF: Simultaneous observations at two altitudes, *J. Geophys. Res.*, *114*, A02311, doi:10.1029/2008JA013624.

Trattner, K. J., S. A. Fuselier, W. K. Peterson, M. Boehm, D. Klumpar, C. W. Carlson, and T. K. Yeoman (2002), Temporal versus spatial interpretation of cusp ion structures observed by two spacecraft, *J. Geophys. Res.*, *107*(A10), 1287, doi:10.1029/2001JA000181.

Trattner, K. J., S. A. Fuselier, S. M. Petrinec, T. K. Yeoman, C. Mouikis, H. Kucharek, and H. Reme (2005), Reconnection sites of spatial cusp structures, *J. Geophys. Res.*, *110*, A04207, doi:10.1029/2004JA010722.

Wild, J. A., et al. (2001), First simultaneous observations of flux transfer events at the high-latitude magnetopause by the Cluster spacecraft and pulsed radar signatures in the conjugate ionosphere by the CUTLASS and EISCAT radars, *Ann. Geophys.*, *19*, 1491–1508.

Wilson, G. R., and T. E. Moore (2005), Origins and variation of terrestrial energetic neutral atoms outflow, *J. Geophys. Res.*, *110*, A02207, doi:10.1029/2003JA010356.

Wing, S., P. T. Newell, and J. M. Rouhoniemi (2001), Double cusp: Model prediction and observational verification, *J. Geophys. Res.*, *106*(A11), 25,571–25,593.

Weiss, L., P. Reiff, E. Weber, H. Carlson, M. Lockwood, and W. Peterson (1995), Flow-aligned jets in the magnetospheric cusp: Results from the Geospace Environment Modeling Pilot Program, *J. Geophys. Res.*, *100*(A5), 7649–7659.

M. R. Collier and T. E. Moore, NASA Goddard Space Flight Center, 8800 Greenbelt Road, Code 670, Greenbelt, MD 20771, USA.

K. Hosokawa and S. Taguchi, Department of Information and Communication Engineering, University of Electro-Communications, 1-5-1 Chofugaoka, Chofu, Tokyo 182-8585, Japan. (taguchi@ice.uec.ac.jp)

Y. Ogawa, N. Sato, S. Suzuki, and A. S. Yukimatu, National Institute of Polar Research, Tokyo 173-8515, Japan.